

Gas-bearing sands appraisal for Zamzama gas field in Pakistan through inverted elastic attributes assisted with PNN approximation of petrophysical properties

Zahid U. Khan^{1,2,*}, Mona Lisa¹, Muyassar Hussain^{1,2}, Syed A. Ahmed^{1,2}

¹ Dept. of Earth Sciences, Quaid-I-Azam University,
Islamabad, Pakistan

² LMK Resources (Private) Limited,
Islamabad, Pakistan

*Corresponding author: zahidkhan680@yahoo.com

Abstract

The Pab Formation of Zamzama block, lying in the Lower Indus Basin of Pakistan, is a prominent gas-producing sand reservoir. The optimized production is limited because of water encroachment surrounding the gas-producing wells, thus it is required to distinguish the gas-sand facies from the remainder of the wet sands and shales for additional drilling zones. An approach is adopted based on the relation between petrophysical and elastic properties to characterize the prospect locations. Petro-elastic models (PEMs) for the identified facies were generated to distinguish lithologies in their elastic ranges. Several elastic properties, including p-impedance (11,600-12,100 m/s*g/cc), s-impedance (7,000-7,330 m/s*g/cc), and Vp/Vs ratio (1.57-1.62), were calculated from the simultaneous prestack seismic inversion (SPSI), allowing the identification of gas sands in the field. The inverted elastic attributes and well-based lithologies were incorporated into the Bayesian framework to evaluate the probability of gas sands. To determine the reservoir quality, bulk volumes of PHIE and clay were estimated using elastic volumes trained on well logs by employing Probabilistic neural networking (PNN), which effectively handles heterogeneity effects. The results showed that the channelized gas sands passing through the existing well locations exhibited reduced clay content and maximum effective porosities of 9%, confirming the reservoir's good quality. Such approaches can be widely implemented in producing fields to completely assess lithofacies and achieve maximum production with minimal risks.

Keywords: Bayesian classification; elastic attributes; petro-elastic models (PEMs); probabilistic neural networking (PNN); simultaneous prestack seismic inversion (SPSI).

1. Introduction

The Zamzama gas field covers the western portion of Kirthar Foredeep (Figure 1a), a part of the Kirthar Fold and Thrust Belt (Ehsan *et al.*, 2018). It is situated in the Lower Indus Basin among several major gas fields (Figure 1b). The Zamzama anticlinal structure resulted due to the collision of the Indian and Eurasian tectonic plates resulting in a significant N-S directed thrust fault (Figure 1c). The 3D seismic mapping and Gas-Water-Contact (GWC) measurements from

the initial discovery well at Zamzama-01-ST1 verified a 300m gas column with 3Tscf in the Pab Formation (Jackson *et al.*, 2004).

The Zamzama gas field produced 1.7Tscf gas; however, lateral ramps connecting the hanging and footwall caused differential water encroachment and pressure depletions in the gas producing wells. GWC is still found deeper in the crestal portions, and new wells can be drilled (Zafar *et al.*, 2018). Accurate mapping of gas-bearing sand facies may be considered risky for using conventional methods. Consequently, seismic reflection interpretation is linked with wells to generate petro-elastic relationships that quantitatively discriminate gas and wet sands (Al-Sulaimi & Al-Ruwaih, 2004). The advanced techniques such as SPSI produce reservoir elastic properties that effectively highlight hydrocarbons in the active fields, such as Niger delta Sandfish (Adesanya *et al.*, 2021), Lower Wilcox lowstand sand deposits along the Texas Gulf Coastal Plain (Zhang *et al.*, 2020), etc.

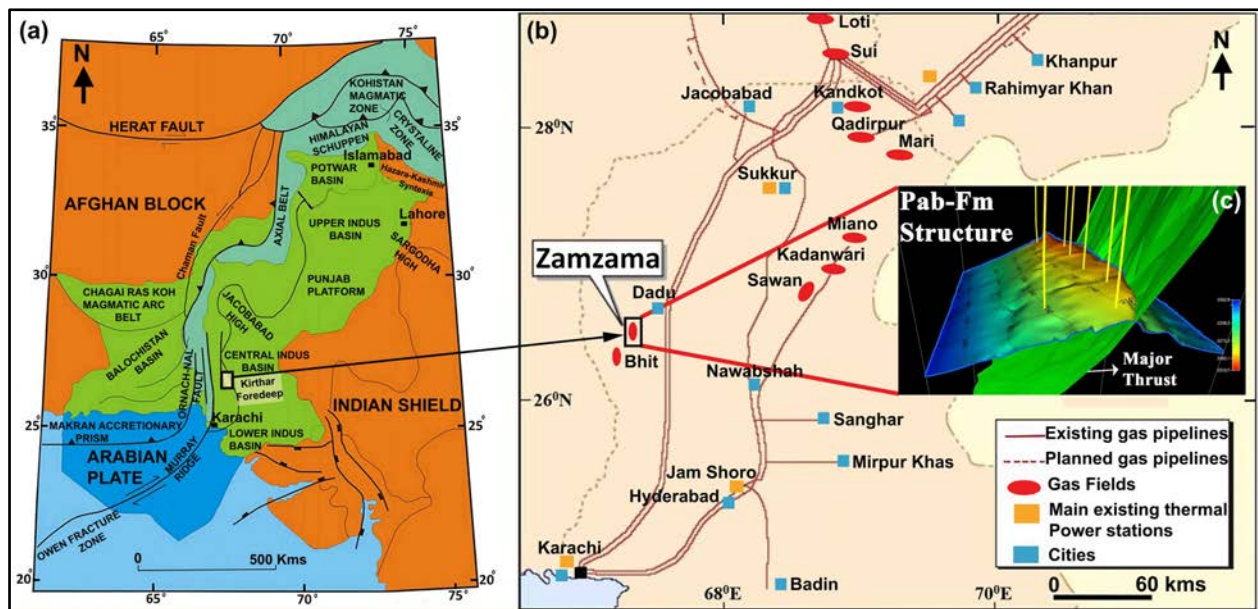


Fig. 1. (a) The regional map highlighting Zamzama field location and demarcating main structural features, (b) The Zamzama region is surrounded by major gas fields, and (c) The anticline of the Pab Formation is cut by a major thrust fault, and wells penetrate it.

Before the seismic inversion, the elastic values of gas-bearing sand facies are analyzed from hard constraint well data. The PEMs combine geology and reservoir parameters to determine elastic responses that differentiate facies and assist in quantitative interpretation (Miraj *et al.*, 2021). For petrophysical distributions (porosity and clay), PNN was used to better manage shales inside sands (Durrani *et al.*, 2020). The main aims included de-risking of new drilling points and improved reserve scheming through integrated geophysical exploration techniques (Li *et al.*, 2020).

2. Methods and techniques

The basic dataset is a 3D seismic cube with seven wells (Zamzama-02, Zamzama-03, Zamzama-04, Zamzama-05, Zamzama-06, Zamzama-07, and Zamzama-08-ST02), produced from the Pab Formation (Figure 2a). Well data included well tops, raw logs, mineralogy, and reservoir in-situ properties. All wells were used in the SPSI process and PNN approximation, while the gas-sands probability was assessed without Zamzama-04 and Zamzama-07 to confirm the high probability in gas-producing locations. Figure 2b delineates a petro-elastic relation in estimating pay probability and PNN approximation of petrophysical properties for Pab gas-sands characterization.

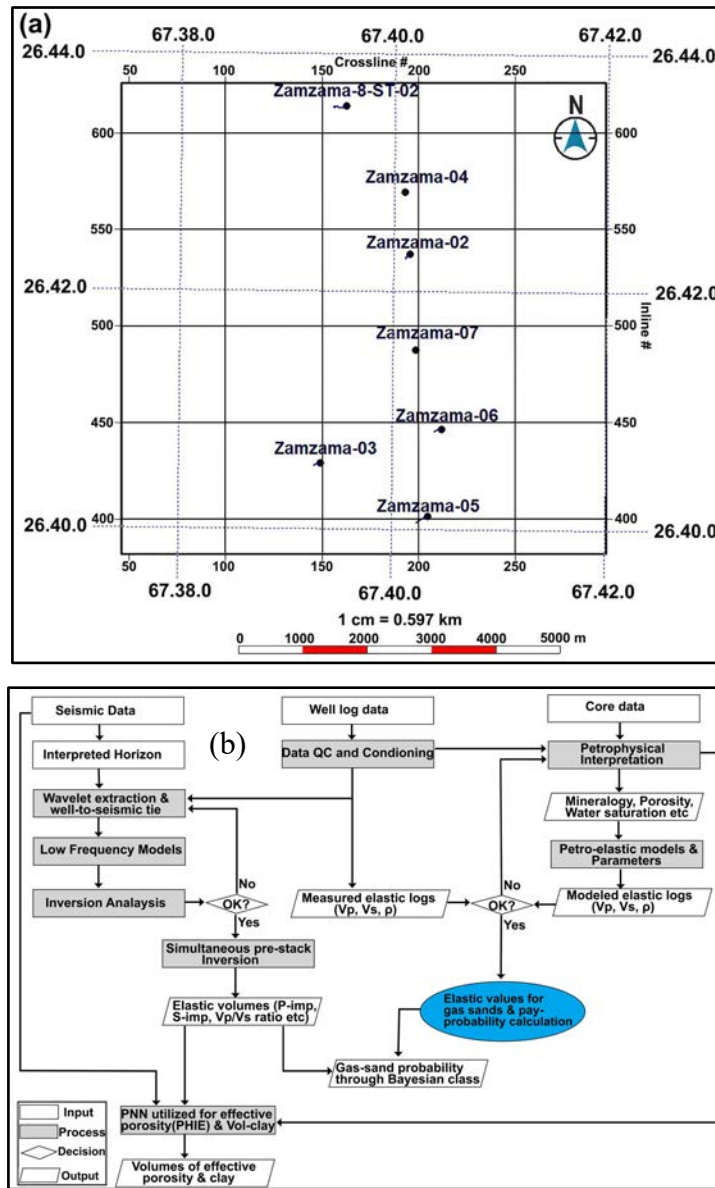


Fig. 2. (a) Base map showing wells and 3D seismic, (b) Workflow with a petro-elastic relation for discriminating gas sands based on estimated pay-probabilities and petrophysical properties.

Lithological identifications are made using cut-off values on petrophysical logs (Table 1). These lithofacies (shale, wet, and gas sands) among reservoir properties were used in PEMs to model consistent elastic logs.

Table 1. Identified lithofacies based on petrophysical cut-off values.

Litho-facies	Cut-off Values
Shale	Clay Volume >0.30
Wet Sands	Clay volume ≤ 0.30 , Sw ≥ 0.45
Gas Sands	Clay volume ≤ 0.30 , Sw < 0.45

The SPSI method includes the interpreted horizons, accurate well-to-seismic tie, strata models of low frequencies (LFMs), and inversion analysis. The output inverted elastic volumes can be calibrated for gas-sands appraisal following the value ranges of modeled elastic logs. Furthermore, the modeled logs relate to the inverted elastic properties in the Bayesian framework for litho-cubes probability estimate. To predict petrophysical volumes, the seismic and inverted volumes were integrated and trained on petrophysical logs using PNN.

2.1 Petro-elastic models (PEMs)

The logs encountered a variety of errors, including poor borehole conditions, washouts, and the invasion of mud filtrates (Zeb & Murrell, 2015). The reliable PEMs, developed using HampsonRussells software, overcame the errors and hence delineated the facies according to their elastic ranges.

PEMs signified elastic responses from petrophysical parameters (lithologies, Sw, porosities), reservoir in-situ conditions (salinity, pressure, temperature), and their association with seismic data (Singha & Chatterjee, 2017). Individual PEMs for the identified facies were created by combining the rock matrix bounds of Voigt (1928) with the reservoir-fluid properties of Batzle & Wang, 1992 substituted by the Gassmann (1951) relation.

The mineral volumes with bulk and shear moduli were selected according to Avseth *et al.* (2005). For K_{dry} calculation, the concept of pore-space stiffness compressibility worked well to manage a limited number of reservoir input parameters (Babasafari *et al.*, 2020). The selected granular model considered porosities between zero and a critical value, i.e., 20% for Pab Formation (Han *et al.*, 1986), and separated the load-bearing sands from grains and fluid suspension.

Figure 3 reveals the petrophysical evaluation of Zamzama-03 for key properties, such as volumetrics, lithologies, porosities, saturations, etc., whereas Table 2 summarizes the parameters used in PEMs.

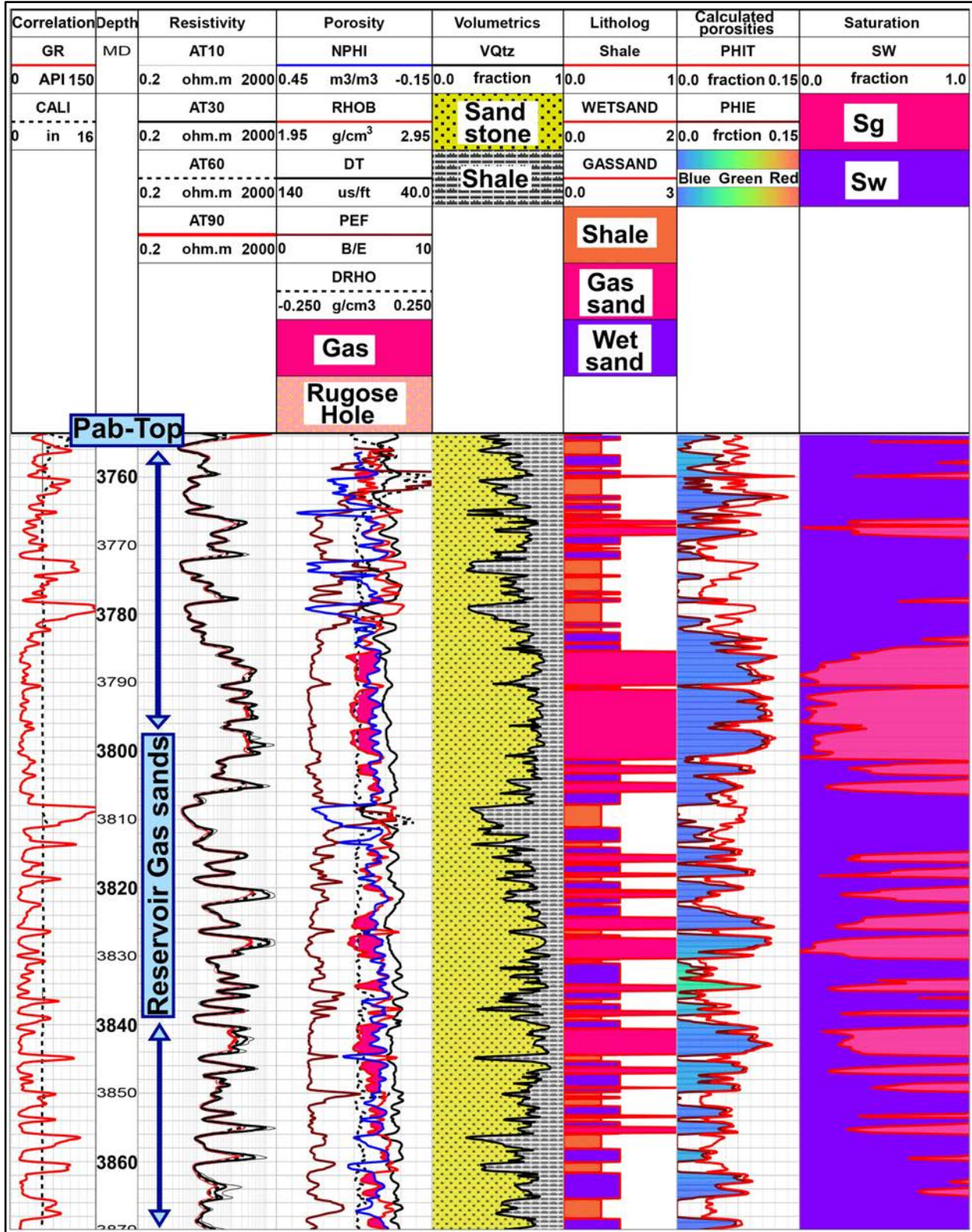


Fig.3. The petrophysical analysis for reservoir Pab Formation (3750-3870m) showing volumetrics, lithologies, calculated porosities, and saturations in their respective tracks.

Table 2. Reservoir petrophysical and elastic properties are utilized in PEMs.

Reservoir Parameters	Avg. Porosity	Avg. Shale	Avg. Water (Sw)	Pressure (PSI)	Temp °C	Salinity (g/l)	Gas gravity					
Values	10%	25%	45%	3400	130	0.15	0.689					
Elastic Parameters	Bulk Modulus (GPA)				Shear Modulus (GPA)				Density (g/cm ³)			
	Quartz	Clay	Sw	Gas	Quartz	Clay	Sw	Gas	Quartz	Clay	Sw	Gas
Values	37	15	2.38	0.02	44	7	0	0	2.65	2.6	1.0	0.1

The modeled elastic logs show consistency with measured logs, i.e., V_p , V_s , and density in the identified lithologies within Pab Formation (Figure 4a). Additional QC was performed in quantitative QC plots of measured vs modeled logs (Figure 4b). The prediction quality (PQ) is 0.94, 0.86, and 0.84 in the cross plots of V_p , V_s , and density, respectively. The correlation coefficient (CC) quantified log values ranging from -1 (anticorrelation) to 1 (perfect correlation) and denoted 0.88, 0.74, and 0.70 in respective cross plots. Similarly, normalized root mean square error (NRMSE) dealt with the degree of difference, with 0 for identical curves and 2 for the greatest difference, indicating 0.07, 0.13, and 0.03 respectively. The log value range was represented by a histogram and the data point size showed its density. This analysis provides confidence in the selected PEMs because all the QC plot values were within reasonable ranges.

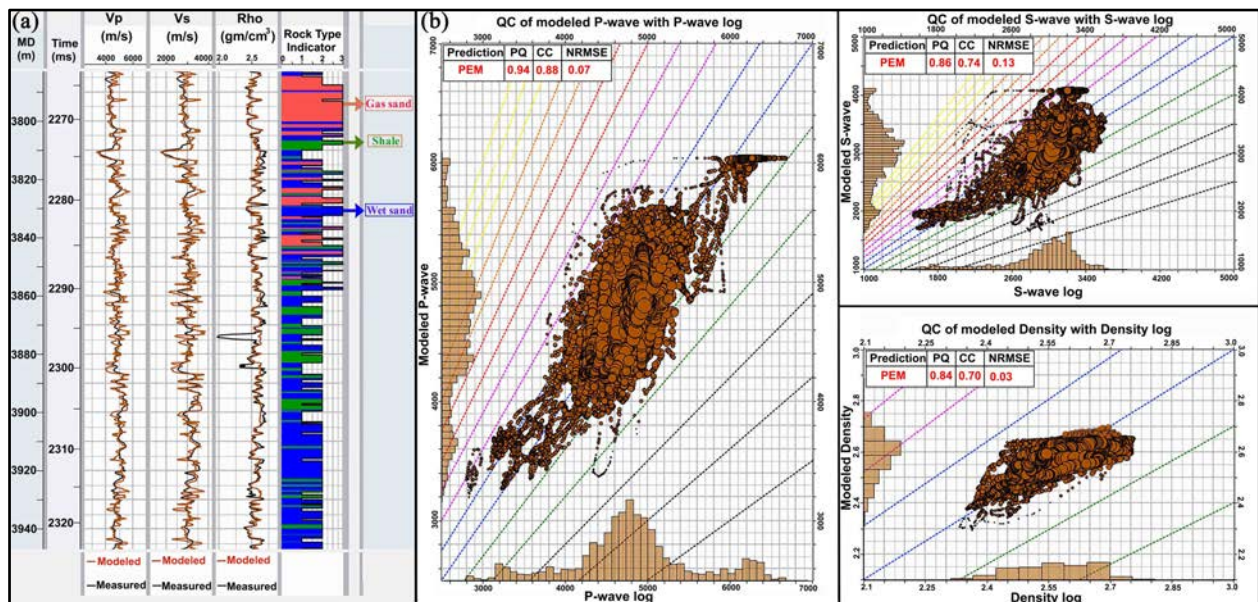


Fig. 4. (a) Modeled logs are overlaid on measured logs with a good fit of trends, (b) The coherence of selected PEMs is demonstrated by the in-range values of quantitative QC plots of real and modeled V_p , V_s , and density.

2.2 Strata Model

The Strata Model, created using HampsonRussells strata module (version 10.6), is a geologic model that uses interpreted horizons, stratigraphic pattern interpolation, and well logs. The seismic data is lacking in low frequencies due to its band-limited nature (Figure 5a). The models incorporate the missing low frequencies from well logs, calculated using the kriging interpolation method, to obtain the absolute elastic properties of seismic (Sams & Saussus, 2013). LFMs (8Hz) acted as background information and were updated with high frequencies in the inversion algorithm (Sams & Carter, 2017). LFMs showed a reliable correlation with low-pass filtered well logs (Figure 5b).

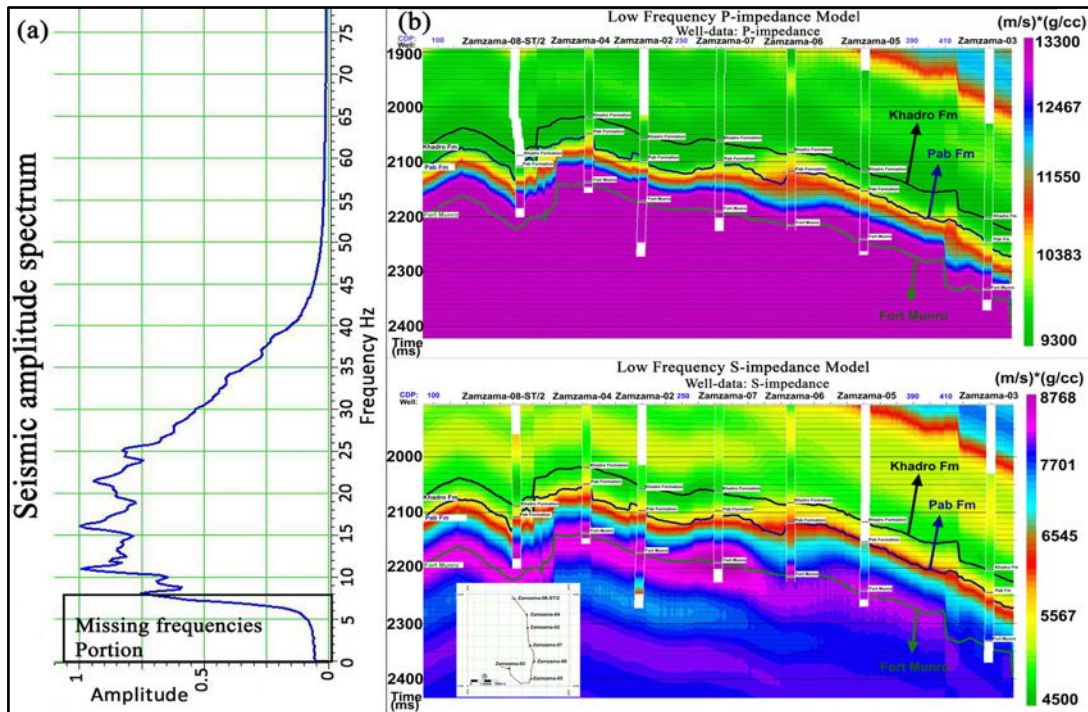


Fig. 5. (a) Seismic spectrum delineating missing low frequencies, (b) LFMs of P and S-impedances with low-pass filtered well logs provided background trend and updated with high frequencies in the inversion process.

2.3 Simultaneous prestack seismic inversion (SPSI)

The LFMs were incorporated into the prior model in SPSI inversion to outline the background trend in inversion analysis. Inversion analysis is a key process that detects discrepancies between inverted and measured logs as errors at well locations.

A reliable comparison of LFMs, well logs, and inverted logs are displayed in the Z_p , Z_s , and V_p/V_s ratio tracks (Figure 6). The inverted logs were utilized to generate synthetic by convolving an extracted angle gathers wavelet and for comparison with seismic data. A good correlation of 0.93 between synthetic and seismic angle gather was achieved with a residual error of 0.3654.

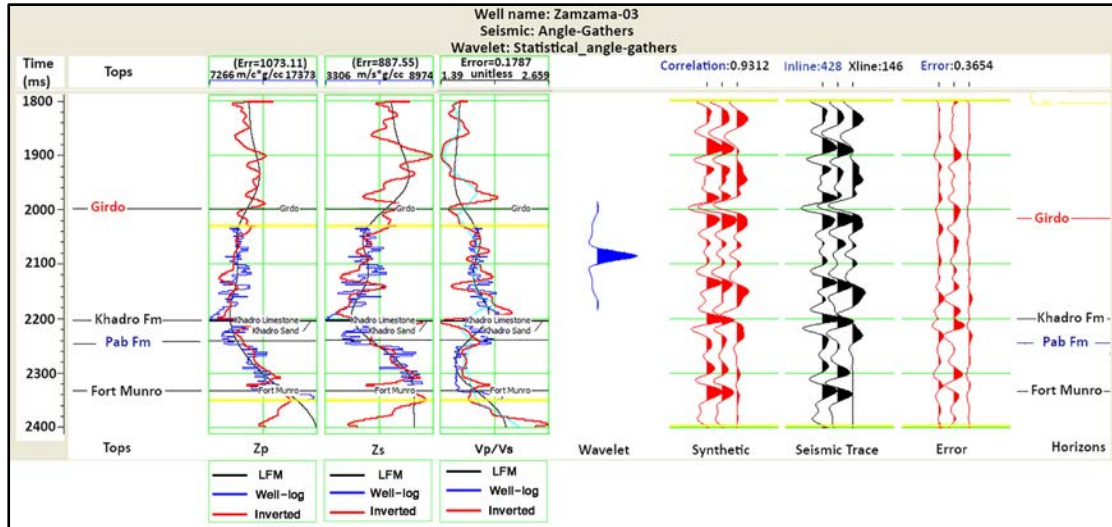


Fig. 6. LFMs are used as background trends in wells and inverted logs comparison. Synthetics (red) and seismic (black) traces provide a correlation of 0.9312 with an error of 0.3654.

The seismic inversion consists of modeling the seismic traces by a 1D convolutional model, utilizing a recursive equation (Russell & Hampson, 1991). For prestack seismic data with different incident angles (θ), an updated version is used in SPSI defined by Fatti *et al.* (1994). The process suggests a constant V_p/V_s ratio with the density estimation using Gardner *et al.* (1974) relation. Hampson *et al.* (2005) incorporated the clastic rocks as background trends (LFMs) in Fatti's equation along with establishing a linear relationship between different logarithms of elastic properties. The linear models fitted to the values of the background trend used p-impedance (Z_p), s-impedance (Z_s), and density (ρ) to calculate the change in the s-impedance (ΔL_s) and density (ΔL_D) that indicated the hydrocarbon presence (Cataldo & Leite, 2018). Figures 7a & b demonstrate ΔL_s and ΔL_D for Zamzama wells indicating gas presence.

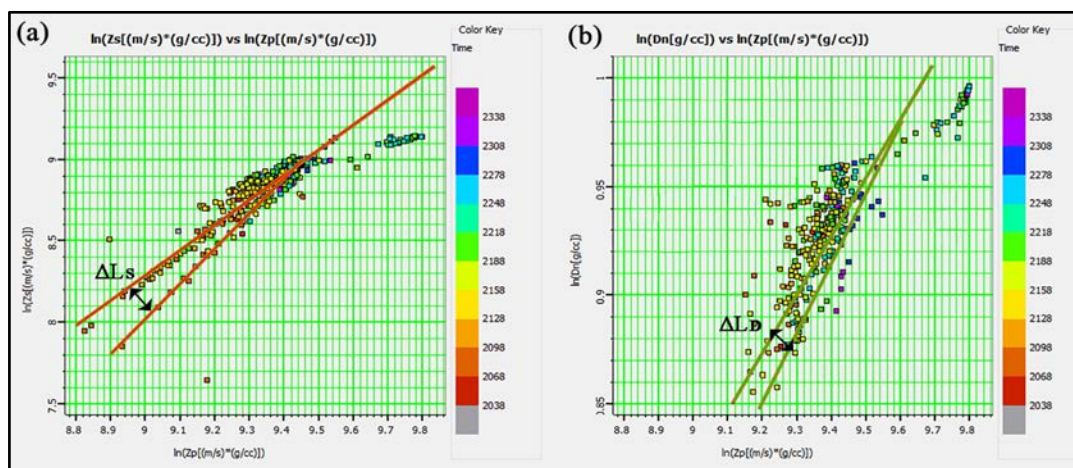


Fig. 7. (a) ΔL_s derived from $\ln(Z_s)$ vs. $\ln(Z_p)$, (b) ΔL_D derived from $\ln(D_n)$ vs. $\ln(Z_p)$. The deviations ΔL_s and ΔL_D from the background trend indicated the presence of gas anomalies in the field.

Finally, the seismic angle gathers inverted through matrix inversion technique $[L_P \ \Delta L_S \ \Delta L_D]^T = [\ln(Z_{P0}) \ 0 \ 0]^T$, in which Z_{P0} represented initial impedance and afterward iterated to get solution by the conjugate gradient method (Hampson *et al.*, 2005). For QC, the inverted p-impedance (Z_p) and s-impedance (Z_s) were compared to the corresponding well logs, indicating a good correlation within Pab Formation (Figures 8a & b).

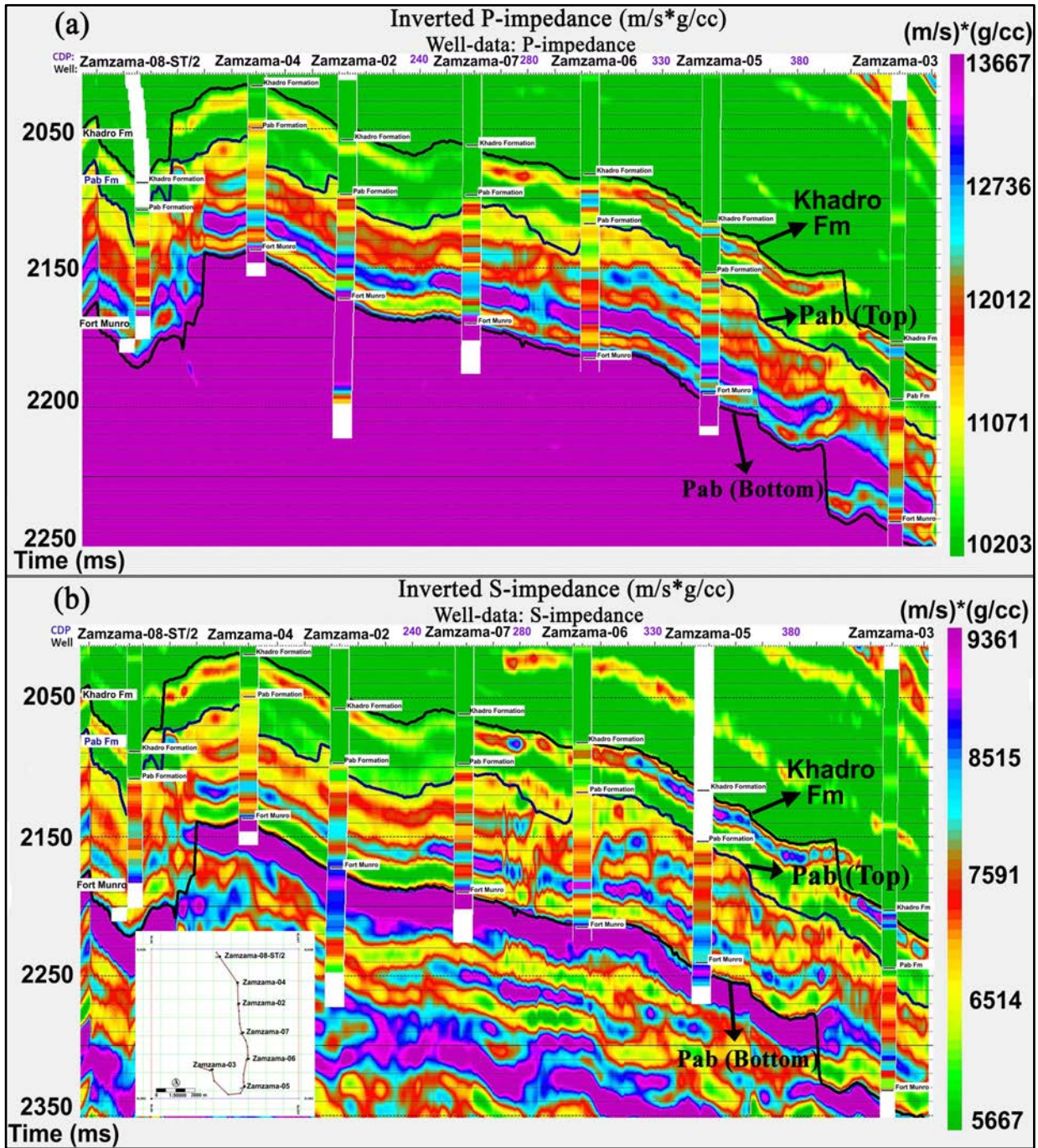


Fig. 8. (a) Inverted p-impedance, (b) Inverted s-impedance, depicting decent correlation with well logs, while the arbitrary line passes through all wells (index map).

2.4 Bayesian probability estimation

Several forms of information, such as petrophysics, seismic characteristics, and subsurface geological knowledge, are combined into the Bayesian framework to obtain reliable pay probability information. Equation (1) is the mathematical expression of the Bayes theorem.

$$p(c_i|X) = \frac{[p(X|c_i)*p(c_i)]}{p(X)} \quad (1)$$

The c represents the class (gas sands), X signifies the inverted elastic properties (Z_p and V_p/V_s ratio) (Figure 9a), and $p(c)$ reflects the prior probability of class as identified from wells (Figure 9b). For multiple distributions, probability density functions (pdfs) are computed on the Z_p and V_p/V_s ratio cross plot using the kernel density estimation approach in the Bayes inference (Figure 9c). The mathematical measure for overlapping and the degree of separation of pdfs between the classes is cross-validated through a confidence matrix that provides classifier-success information. The confidence matrix reveals the probability of obtaining the target facies, i.e., gas sands (89.5%) from upscaled logs. The upscaled lithofacies logs, which resulted from the pdfs computation on a 2D cross plot, showed an acceptable correlation with the lithologies of the well (Figure 9d). In this process, five wells were utilized, while two operational wells Zamzama-04 and Zamzama-07 were tested for gas-bearing sand facies without incorporating them in this procedure. The output gas-sand probability within the Pab Formation was extracted through all available wells having GR logs depicting potential zones at the gas-producing well locations (Figure 9e).

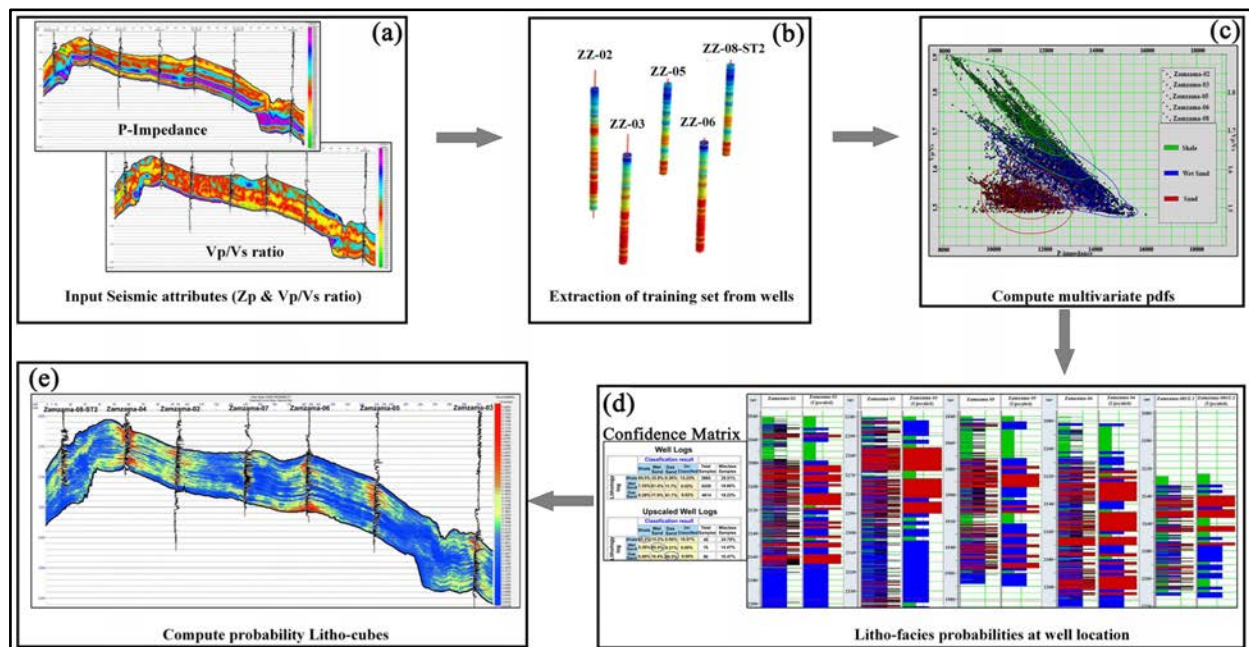


Fig. 9. (a) Inverted p-impedance and V_p/V_s ratio within Pab Formation, (b) Well-based facies and logs utilized as training set, (c) PDFs of identified facies, (d) Upscaled lithologies of pdfs and confusion matrix, and (e) Estimated gas-probability passing all the wells.

3. Probabilistic neural networking (PNN) approximation

The accurate estimation of reservoir properties away from well is one of the critical aspects of reservoir characterization. The linear and multi-linear regression analyses were adopted for the relation between petrophysical and elastic properties (Lorenzen, 2018). However, their reliability can be limited due to variations in the reservoir properties. The advancement in computational technology suggests non-linear relations for solving complex problems even for shale plays without any prior information (Durrani *et al.*, 2020). The PNN is a non-linear interpolation mathematical procedure explained in detail by Sinaga *et al.* (2019), which trains the input petrophysical logs with internal (sample-based seismic volume) and external attributes (impedances and Vp/Vs ratio). The internal attributes are generated by mathematical transforms on seismic amplitudes, including trace envelope, amplitude weighted cosine phase, amplitude weighted frequency, and instantaneous phase, while external attributes include inverted elastic properties or AVO attributes.

The clay volume is trained at well locations within Pab Formation using PNN (Figure 10a). A good agreement of predicted and actual logs could be observed having a correlation coefficient of 0.9161 with an error of 0.0489. The cross plot confirms the match of trends by setting a regression line (Figure 10b). The estimated clay volume is passing through all wells, filled with colored clay logs for the QC of the estimated volume (Figure 10c).

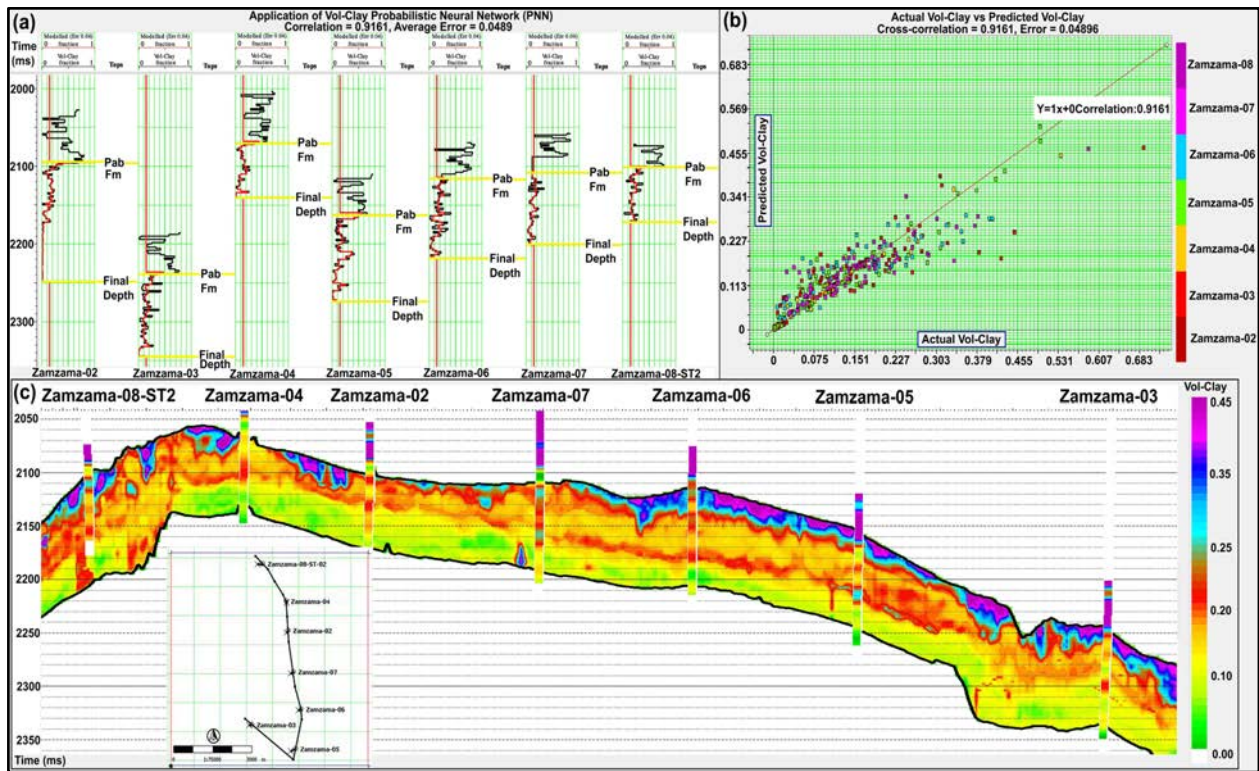


Fig. 10. (a) At the well sites, clay volume is trained using PNN, (b) Regression line showing correlation of 0.9161, and (c) Estimated clay volume depicts precise match with clay logs.

A similar process was adopted for effective porosity (PHIE) prediction, starting at the well points (Figure 11a). The correlation coefficient of 0.9326 between actual and predicted logs was observed with an error of 0.0118 (Figures 11b). The cross-section of effective porosity volume confirmed decent accordance with PHIE logs (Figure 11c).

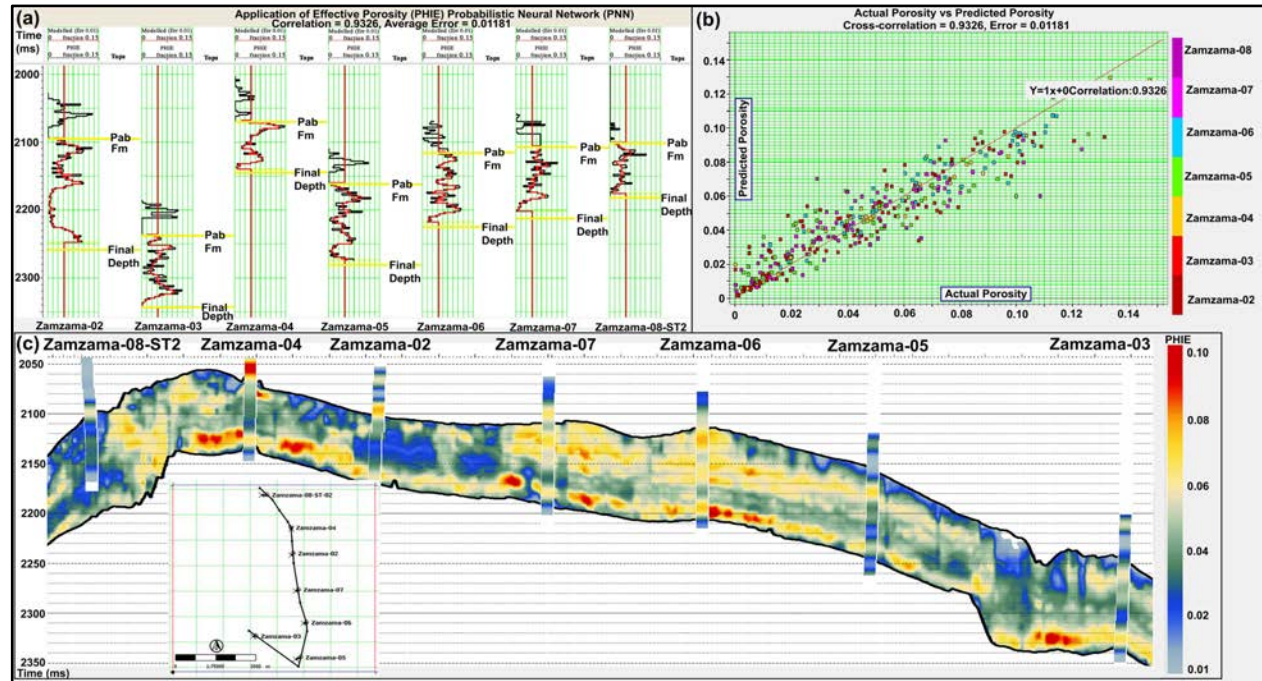


Fig. 11. (a) PNN training of PHIE at wells, (b) Regression line showing correlation of 0.9326, and (c) PHIE volume reveals appropriate match with PHIE logs.

4. Results and discussion

Typically, geologic facies hold a range of elastic values that help in their discrimination (Naeni & Exley, 2017). Certain factors, such as recording tool limitations for managing reservoir heterogeneity, may cause these ranges to overlap as seen in the Zamzam-03 well, where shales, wet, and gas sands are not distinguished (p-impedance versus V_p/V_s ratio) (Figure 12a). In the modeled elastic logs, the elastic values of identified lithofacies are more consistent. Figure 12b shows a good match between the modeled (blue) and measured (red) logs while correcting the outrange density log at 2295m. Figure 12c shows facies separation and the Rock Physics Template (RPT) delineates an acceptable gas quantity of 8-12% of porosities with an inverse relationship to p-impedance (Al-Ruwaih, 1998).

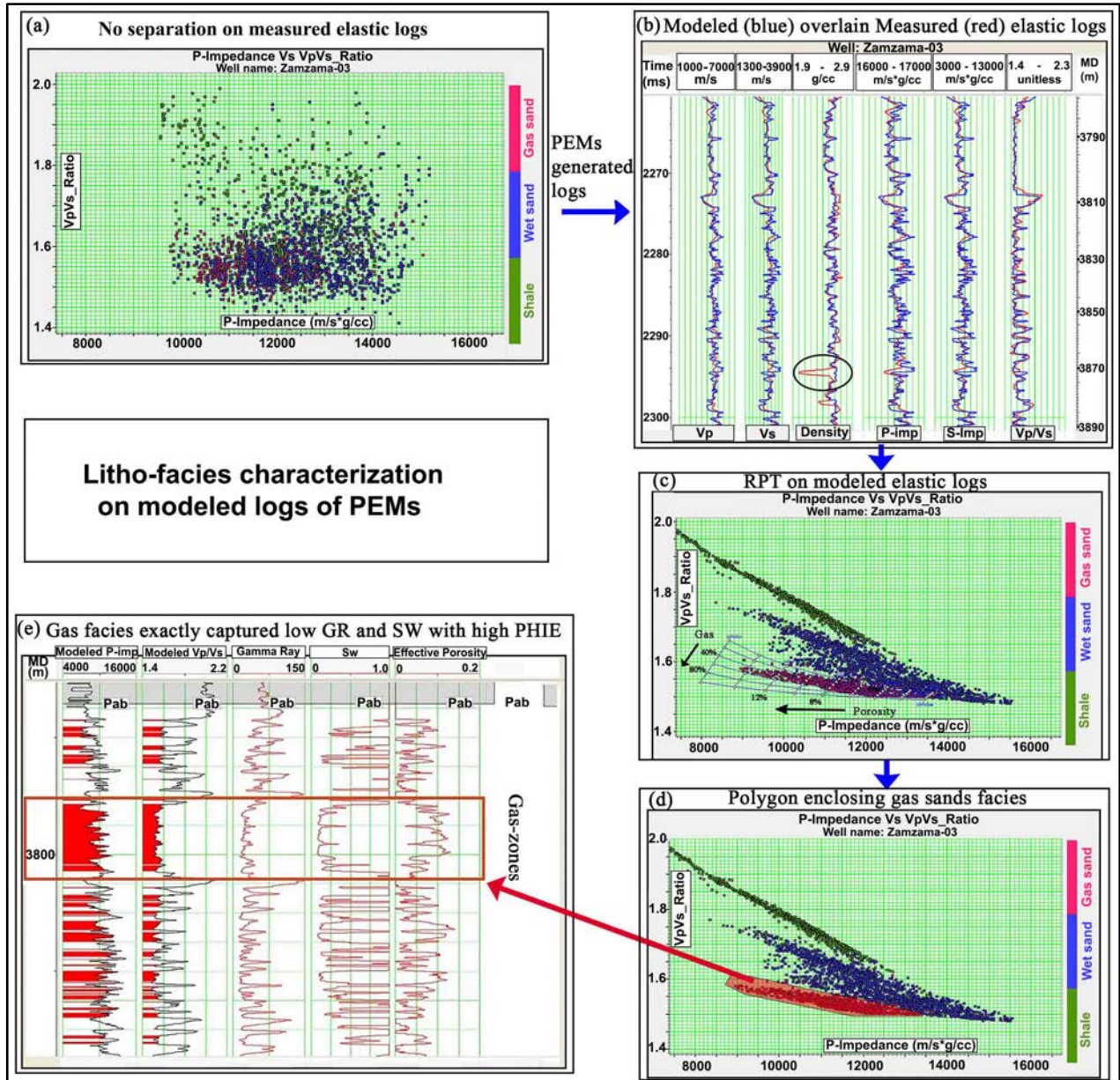


Fig. 12. (a) Mixed lithofacies in measured logs, (b) Modeled logs exhibit trend consistency with measured logs and corrected outrange values, such as the encircled density log at 2295m, (c) RPT captured a significant amount of gas at 8-12% PHIE, (d) Polygon bounding the gas-sands, and (e) Projection of gas sands show low GR, Sw, and high PHIE.

The cross plot provides value ranges of p-impedance (9,000-13,000 m/s*g/cc) and Vp/Vs ratio (1.5-1.62) that aided in the location of gas sands on SPSI inverted volumes. The gas facies are encircled and projected in the well-bore to investigate elastic and petrophysical relationships (Figures 12d). The gas intervals matched the perforation history, evident by low GR and Sw with good effective porosities (Figure 12e).

The stratigraphic maps are generated by averaging the elastic properties (Z_p , Z_s , and V_p/V_s ratio) within the Pab Formation. The P-impedance map, which shows values ranging from 11,600 to 12,100 (m/s)*(g/cc) for all gas-producing well locations, can help to identify prospects in these ranges (Figure 13a). The S-impedance values range from 7,000 to 7,330 (m/s)*(g/cc), suggesting gas sands at the well sites (Figure 13b). The V_p/V_s ratio is significant as several field examples have demonstrated its effectiveness in identifying the fluid types (Hamada, 2004). The V_p/V_s ratio suggests gas-sand facies with values ranging from 1.57 to 1.62 and it passes through all the producing wells, confirming the fairway of the channelized gas-sand body (Figure 13c).

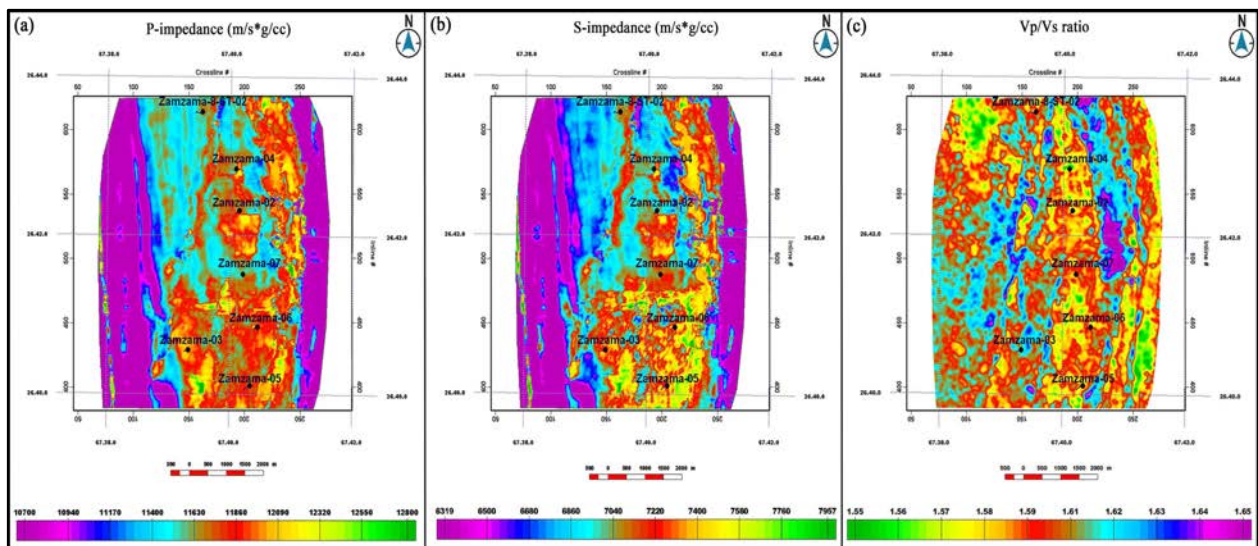


Fig. 13. (a) P-impedance ranges from 11,600 to 12,100 m/s*g/cc at the productive well locations, (b) S-impedance range between 7,000 to 7,330 m/s*g/cc indicates gas-filled sands, and (c) V_p/V_s ratio is less than 1.62 in producing wells, suggesting channelized sands.

The pay-probability map, developed by extracting maximum values inside the Pab Formation, verifies the channelized gas sands at well positions (Figure 14a). The polygons constructed over the high probability zones demarcate channelized gas sands, enclosing zones (north of the Zamzama-03 well) that can be used to assess additional prospect locations. The average valued clay map reflects the cleanliness of the Pab Formation, with a minor clay concentration of about 30% in the major producing crestal section of the anticline structure (Figure 14b). The effective porosity map depicted 9% effective porosities surrounding the operational well locations (Figure 14c). Overall, the Pab Formation comprises majorly of sandstone with low clay volumetrics and fair effective porosities.

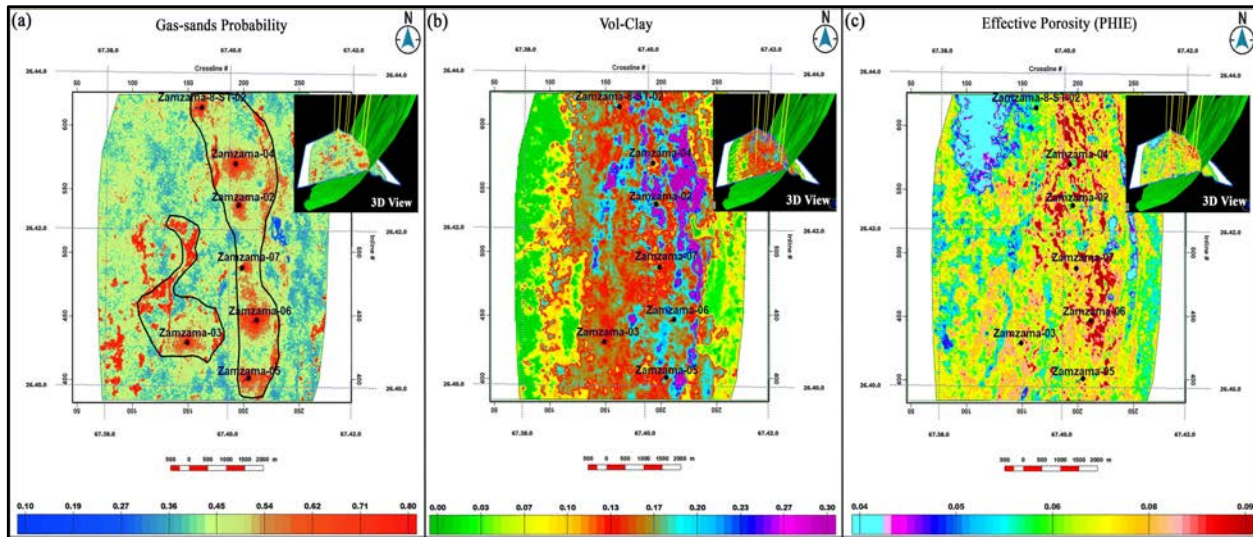


Fig. 14. (a) High probability channelized gas-sand facies encircled by polygons passing through all wells, (b) Clay map confirms good quality of sands having minor clay content, and (c) The 9% effective porosities are present along the operational wells. (The 3D views illustrate the corresponding property distribution with wells penetrating the anticline's crestal zone and a large thrust bisecting the structure).

5. Conclusion

The approach used here included an integrated petro-elastic relation, which resulted in reliable gas-sands prediction with minimum uncertainties. PEMs were used to quantify the gas-sand facies, which were traced on inverted elastic volumes and confirmed by high pay probabilities. The gas-probability map revealed channelized gas sands and highlighted new prospect locations. The prospect areas indicate reduced clay volumetric with maximum effective porosities of 9%, supporting a good sand quality. Such information integration efficiently characterizes the producing facies, allowing the optimal site location for new wells with the lowest risk.

ACKNOWLEDGMENTS

DGPC (Pakistan) provided the data for research, while the software is provided by LMK Resources (Private) Limited, Islamabad, Pakistan, and Compagnie Générale de Géophysique (CGG).

References

Adesanya, O.Y., Adeoti, L., Oyedele, K.F., Afinotan, I.P., Oyeniran, T. & Alli, S. (2021) Hydrocarbon reservoir delineation using simultaneous and elastic impedance inversion in a Niger Delta field. *Journal of Petroleum Exploration and Production Technology*, 11(7): 2891-2904.

Al-Ruwaih, F. M. (1998) Numerical modeling of Umm-Gudair well field, Kuwait. *Kuwait Journal of Science and Engineering*, 25, 231-248.

Al-Sulaimi, J.S. & Al-Ruwaih, F.M. (2004) Geological, structural, and geochemical aspects of the main aquifer system in Kuwait. *Kuwait Journal of Science and Engineering*, 32(1): 149-174.

Avseth, P., Mukerji, T. & Mavko, G. (2005) Quantitative seismic interpretation: Applying rock physics tools to reduce interpretation risk. Cambridge University Press.

Babasafari, A.A., Ghosh, D.P., Salim, A.M.A. & Kordi, M. (2020) Integrating petro-elastic modeling, stochastic seismic inversion, and Bayesian probability classification to reduce the uncertainty of hydrocarbon prediction: Example from Malay Basin. *Interpretation*, 8(3): SM65-SM82. <https://doi.org/10.1190/INT-2019-0077.1>

Batzle, M. & Wang, Z. (1992) Seismic properties of pore fluids. *Geophysics*, 57(11): 1396-1408. <https://doi.org/10.1190/1.1443207>

Cataldo, R.A. & Leite, E.P. (2018) Simultaneous prestack seismic inversion in a carbonate reservoir. *REM-International Engineering Journal*, 71(1): 45-51.

Durrani, M.Z.A., Talib, M., Ali, A., Sarosh, B. & Naseem, N. (2020) Characterization and probabilistic estimation of tight carbonate reservoir properties using the quantitative geophysical approach: A case study from a mature gas field in the Middle Indus Basin of Pakistan. *Journal of Petroleum Exploration and Production Technology*, 10(7): 2785-2804.

Ehsan, M., Gu, H., Akhtar, M.M., Abbasi, S.S. & Ehsan, U. (2018) A geological study of reservoir formations and exploratory well depths statistical analysis in Sindh Province, Southern Lower Indus Basin, Pakistan. *Kuwait Journal of Science*, 45(2): 84-93.

Fatti, J.L., Smith, G.C., Vail, P.J., Strauss, P.J. & Levitt, P.R. (1994) Detection of gas in sandstone reservoirs using AVO analysis: A 3D Seismic Case History Using the Geostack Technique. *Geophysics*, 59(9): 1362-1376. <http://dx.doi.org/10.1190/1.1443695>

Gardner G.H.F., Gardner L.W. & Gregory A.R. (1974) Formation velocity and density—the diagnostic basics for stratigraphic traps. *Geophysics*, 39(6): 770-780. <https://doi.org/10.1190/1.1440465>

Gassmann, F. (1951) Elastic waves through a packing of spheres. *Geophysics*, 16(4): 673-685.

Hamada, G.M. (2004) Reservoir Fluids Identification Using Vp/Vs Ratio. *Oil & Gas Science and Technology*, 59(6): 649-654. <https://doi.org/10.2516/ogst:2004046>

Hampson, D., Russell, B.H. & Bankhead, B. (2005) Simultaneous inversion of pre-stack seismic data. SEG Annual Meeting, Houston, 2015, Abstracts No. 21, Pp. 1633-1637. <https://doi.org/10.1190/1.2148008>

Han, D.H., Nur, A. & Morgan, D. (1986) Effects of porosity and clay content on wave velocities in sandstones. *Geophysics*, 51(11): 2093-2107.

Jackson, M.A., Hill, R., Roberson, P., Woodall, M.A., Wormald, G. & Jafri, N. (2004) Zamzama Gas Field – Balancing Risk and Value. Proceedings of SPE Asia Pacific Oil and Gas Conference and Exhibition, Perth, 18th to 20th October 2004.

Li, Z., LI, Q. & Zhang, H. (2020) Integrated physical detection technology in complicated surface subsidence area of mining area. Kuwait Journal of Science, 47(1): 86-96.

Lorenzen, R. (2018) Multivariate linear regression of sonic logs on petrophysical logs for detailed reservoir characterization in producing fields. Interpretation, 6(3): T543-T553. <https://doi.org/10.1190/INT-2018-0030.1>

Miraj, M.A.F., Ali, A., Javaid, H., Rathore, P.W.S., Ahsan, N., Saleem, R.F., Afgan. & S., Malik, M.B. (2021) An integrated approach to evaluate the hydrocarbon potential of Jurassic Samana Suk Formation in Middle Indus Basin, Pakistan. Kuwait Journal of Science, 48(4): 1-11.

Naeini, E.Z. & Exley, R. (2017) Quantitative interpretation using facies-based seismic inversion. SEG, 5(3): SL1-SL8. <http://dx.doi.org/10.1190/INT-2016-0178.1>

Russell, B. & Hampson, D. (1991) Comparison of Poststack Seismic Inversion Methods. SEG Technical Program, Abstracts No. 10, Pp. 876-878. <https://doi.org/10.1190/1.1888870>

Sams, M. & Carter, D. (2017) Stuck between a rock and a reflection: A tutorial on low-frequency models for seismic inversion. Interpretation, 5(2): B17-B27.

Sams, M. & Saussus, D. (2013) Practical implications of low-frequency model selection on quantitative interpretation results. SEG Technical Program Expanded Abstracts 2013, Pp. 3118-3122. <https://doi.org/10.1190/segam2013-0660.1>

Sinaga, T.M., Rosid, M.S. & Haidar, M.W. (2019) Porosity Prediction Using Neural Network Based on Seismic Inversion and Seismic Attributes. The 4th International Conference on Energy, Environment, Epidemiology, and Information System (ICENIS 2019), E3S Web of Conferences 125, article no. 15006, Pp. 1-5. <https://doi.org/10.1051/e3sconf/201912515006>

Singha, D.K. & Chatterjee, R. (2017) Rock physics modeling in the sand reservoir through well log analysis, Krishna-Godawari basin, India. Geomechanics and Engineering, 13(1): 99-117. <https://doi.org/10.12989/gae.2017.13.1.099>

Voigt, W. (1928) Lehrbuch Der Kristallphysik. Teubner, Leipzig. ISBN: 978-3-663-15884-4, Pp. 962.

Zafar, Z.A., Shoaib, K., Afsar, F., Raja, Z.A., Tanveer, A. & Burley, S.D. (2018) A RADICAL SEISMIC INTERPRETATION RE-THINK RESOLVES THE STRUCTURAL COMPLEXITIES OF THE ZAMZAMA FIELD, KIRTHAR FOREDEEP, PAKISTAN. PAPG/SPE Annual Technical Conference, Islamabad, 11-12 December 2018.

Zeb, J. & Murrell, R. (2015) Evaluation of Rock Properties from Logs Affected by Deep Invasion-A Case Study. The 3rd International Workshop on Rock Physics, Perth, 13th to 17th April 2015.

Zhang, T., Lin, Y., Liu, K.H. & Gao, S.S. (2020) Pre-stack simultaneous inversion for delineation of the Lower Wilcox erosional remnant sandstone beneath the Texas Gulf Coastal Plain: A case study. Interpretation, 8(4): T991-T1005. <https://doi.org/10.1190/INT-2019-0178.1>

Submitted: 27/08/2021

Revised: 16/11/2021

Accepted: 23/11/2021

DOI: 10.48129/kjs.15915